

Semi-analytical approach for plane strain sheet metal forming using a bending-under-tension numerical model

Guénaél Le Quilliec · Piotr Breitung ·
Jean-Marc Roelandt · Pierre Juillard

Received: 5 December 2012 / Accepted: 17 December 2012 / Published online: 27 January 2013
© Springer-Verlag France 2013

Abstract In this paper, we revisit the plane strain deep-drawing process. We show that a detailed analysis of the physical process may result in a dramatic reduction of computing time when the problem is split into several regions undergoing well-defined loading paths. The proposed approach allows us to assess the springback of the formed sheet in a quasi-instant time and is thus suitable in the initial design phase and provides a fast and economical way to determine the influence of the numerous parameters involved in sheet metal forming. We present a semi-analytical model that has been developed for sheet metal forming mainly subjected to plane strain bending-under-tension and involving large strains. The sheet is considered to be an assembly of regions where the loading is considered homogeneous in the length direction. A handful of finite elements or even a single element is sufficient to compute the loading path followed by each region. The contact is circumvented by constraining the kinematics with appropriate boundary conditions and the approach is valid for any material behavior law. The semi-analytical model is applied to standard test cases and then compared with full-scale simulations.

Keywords Sheet metal forming · Springback · Reduced model · Semi-analytical method · Deep-drawing · Plane strain

Introduction

Sheet metal forming is a class of manufacturing processes aiming to permanently deform a sheet metal blank into a desired shape. Deep drawing is one of the most frequently used metal forming techniques. The desired shape is typically achieved through one or more deep drawing operations. As shown in Fig. 1, the blank is placed between the motionless die and the mobile punch. A blank-holder is generally used to clamp the sheet with a controlled force while the punch moves into the die. This device is used in an attempt to prevent tearing and wrinkling defects and helps to control the material flow. In order to increase the tension in the blank during the operation, draw beads can also be used. After the forming phase, additional deformations appear when the loading is removed. This phenomenon, called springback is amplified when using high strength materials, i.e. with a high ratio of yield strength to Young's modulus. The design of tools required to obtain a desired final shape of deep drawn parts requires a precise prediction of springback effect.

Understanding the influence of the numerous parameters involved in such a forming process, by means of experimental trials, and their subsequent analysis, is very long and expensive. Simulations using the finite element method (FEM) can significantly decrease the number of experimental trials as shown by Da Silva Botelho et al. [9]. Such models are often used in the optimization of deep drawing processes. Breitung et al. [4] shown the accuracy of moving last square approximation in sheet metal forming

G. Le Quilliec (✉) · P. Breitung · J.-M. Roelandt
Laboratoire Roberval, UMR 7337 UTC-CNRS,
Université de Technologie de Compiègne,
60205 Compiègne, France
e-mail: guenael.le-quilliec@utc.fr

P. Juillard
Automotive Steel Solution Design,
ArcelorMittal, Global Research and Development,
60761 Montataire, France

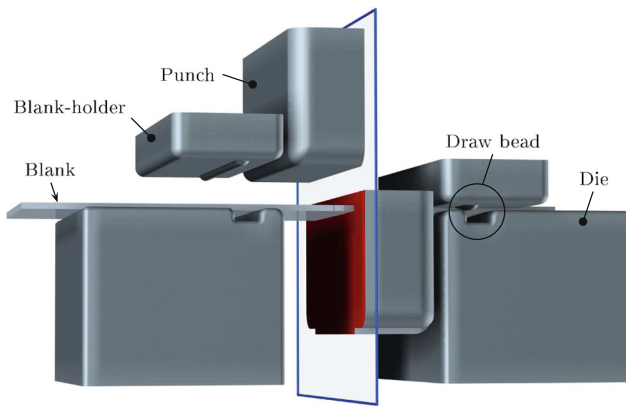


Fig. 1 Schematic example of deep drawing device

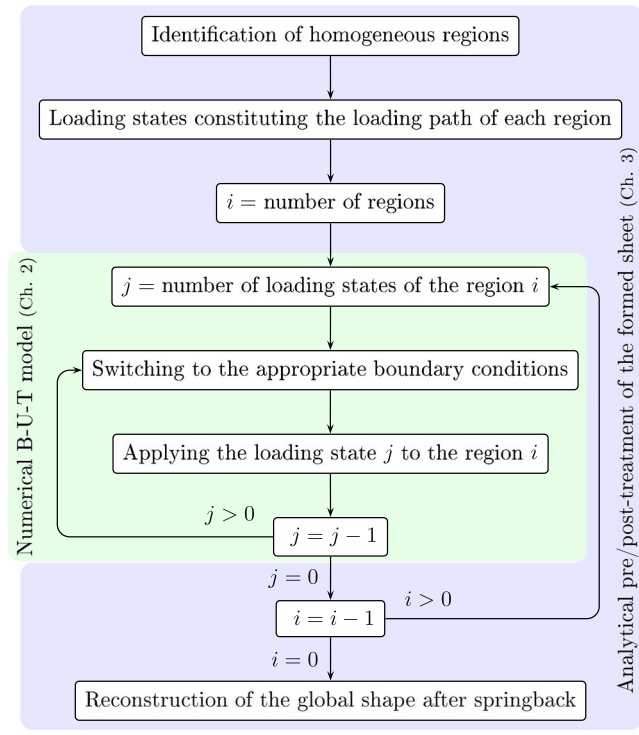
optimization. Sun et al. [19] decreased the computational cost by combining two models with two different fidelity levels to construct the surface response. However, performing a series of simulations of deep drawing is still time consuming, mainly due to the friction contact, need for refined meshes, numerous incremental steps, and slow convergence. Thus, some alternative numerical approaches dedicated to sheet metal forming have been developed. The Inverse Approach [16] is a general way to compute an approximate solution in a single step but still uses a full-scale modeling of the sheet. For 2D plan strain deep drawing, reduced models provide a more economical alternative in the initial design phase. They are generally based on analytical or semi-analytical approaches. For instance, Asnafi [3] proposed an analytical model to predict springback in v-die air bending. Buranathiti and Cao [7] developed an other analytical model dedicated to a straight flanging process. Zhang et al. [20] proposed an analytical model able to approximate springback for a U-shaped sheet. All these analytical approaches are limited to plane strain problems and consider a simple bending-under-tension loading type to approximate the springback geometry. Many analytical models of plane strain pure bending have been developed in the literature surveyed. Hill [12] proposed the first analytical model of pure bending assuming perfectly plastic behavior. Bruhns et al. [6] proposed an elastic-plastic model with combined isotropic and kinematic hardening law. Zhu [21] developed an other model based on power-law-hardening. Hwang [1] took into account the plastic anisotropy behavior of the sheet in their pure bending analytic model. Other analytical methods have been extended to plane strain bending-under-tension that could be used for plane strain metal forming analytical approaches. Parsa and Nasher Al Ahkami [17] considered an elastic-work hardening material in their analytical model of bending-under-tension. More recently, Alexandrov et al. [2] proposed an analytical model of an isotropic incompressible sheet subjected to large strains bending-under-tension considering

quite an arbitrary hardening law based on Tresca yield function. However, while time-saving, those analytical models are also more restrictive and generally limited to conditions of isotropic behavior, specific elastic-plastic hardening law, Tresca yield function, small strain assumption, no thickness thinning, linear through-thickness strain evolution, incompressible material, no multiple reverse bending or Bauschinger effect, etc. Semi-analytical methods are generally less restrictive. The general semi-analytical approach developed by Pourboghrat et al. [18] consists, in a first step, to perform a finite element simulation with a membrane model corrected analytically, in a second step, to superpose bending stretches. Lee et al. [14] used this approach to predict springback in plan strain draw bend test.

In the present work, we focus on 2D plane strain forming process with negligible shear stresses. Many forming processes can be considered as being in plane strain state, such as sheet metal folding, wiping, roll bending, etc. The overall idea of our proposed approach is to split the domain into a set of subdomains subjected to different states of bending and tension loadings. The analysis of an individual domain requires a finite element representation of a single typical section involving thus a column of 2D/3D solid elements, or even a single beam or shell element, whose kinematics is constrained by properly defined boundary conditions. We thus replace a 2D model by a set of uncoupled 1D counterparts, resulting in significant saving of CPU time. It must be noted that the boundaries of the subdomains do not need to be known a priori. Only the number of zones and their respective loading path must be defined by the user. Finally, the deformed shape after springback is reconstructed based on the deformations of the individual sections. We thus combine an analytical approach with the full set of possibilities offered by modern finite-element codes (material laws, kinematics) applied to a set of small-scale problems, while avoiding time-consuming issues such as dealing with a high number of finite elements and modeling friction contact.

The main steps of the present approach are reported in Algorithm 1. In the next section, we propose a finite element model of plane strain bending-under-tension (B-U-T) aimed at circumventing the limitations of the usual analytical as well as numerical (FE) methods. The numerical bending-under-tension model is used in section “[Analytical part: from the B-U-T model to the deep drawing model](#)” as a basis of a semi-analytical forming model for the assessment of deep-drawn sheet, and more specifically for springback prediction. Finally, in section “[Application of the proposed approach](#)”, the presented approach is applied to two classical test cases. The predicted shapes after springback are compared to the reference results obtained from a complete modeling of the two considered metal forming cases.

Algorithm 1 Main steps of the proposed semi-analytical plane strain deep-drawing approach.



Numerical part: bending-under-tension finite element model

We consider a flat sheet submitted to bending-under-tension loading. We propose to establish a numerical solution of this problem, for an arbitrary behavior law, considering large plane strain. The model should be able to impose a given tension combined with a given bending moment or with a given bending radius.

Figure 2 shows the initial and loaded states of the considered sheet. The sheet width W_s has to be sufficiently wide in order to respect the plane strain assumption. Material properties are considered homogeneous in the length direction. Flat sections perpendicular to the initial mean surface remain flat and perpendicular to it under loading since no shear stress is involved. Even if large strains occur, the sheet state under such a loading theoretically remains homogeneous in the length direction. Its shape can be characterized at any time by the bending angle A , the lower side radius r_a and the upper side radius r_b . The radius r_m corresponds to the mean radius, whereas r_n corresponds to the neutral surface one, that is:

$$r_n = \frac{L_0}{A} \tag{1}$$

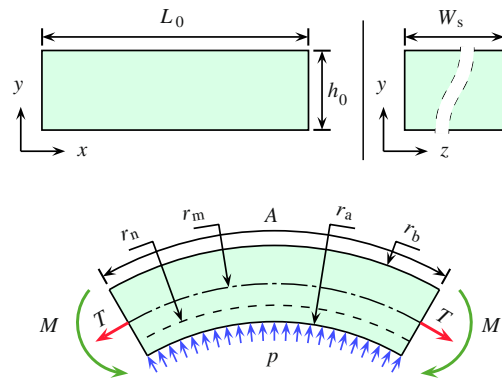


Fig. 2 Scheme of the initial and deformed states of a sheet under finite plane strain bending and tension loading

Following convention, the parameters A , r_n , r_m , r_a and r_b are considered positive when the axe of bending is located in the lower side.

Due to the length homogeneity, it is sufficient to model only a slice of initial length $l_0 \ll L_0$ (Fig. 3). Knowing the state of this slice, it is possible to deduce the complete state of the loaded sheet. The tension is imposed in terms of mean effort T through the slice section. The bending is controlled in terms of a given moment M or a bending radius such as r_n , r_m , r_a or r_b . By analogy with Eq. 1, r_n is also linked to α by:

$$r_n = \frac{l_0}{\alpha} \tag{2}$$

At this point the bending-under-tension problem is fully defined and needs to be solved using a finite element code. The choice of the code is left free to the user and in general case will be guided by availability of constitutive model, finite element formulation (volume/surface) and finally the facility of implementation and switching between different boundary conditions (these issues are discussed in detail in following sections) during the loading/unloading phases.

To simplify the programming of such a combined loading, the tension is maintained constant when the bending loading varies and vice versa. The loading path to be followed is split into a sequence of loading states. All the loading states computed in our finite element model are

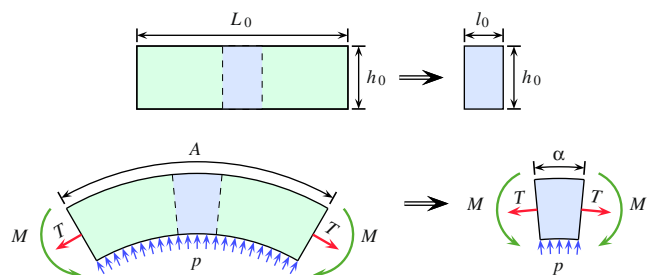


Fig. 3 Scheme of the initial and deformed states of a given slice of the complete sheet

Table 1 Loading states compatible with the developed finite element model

Loading state	1	2	3	4	5	6	7 ^a	8	9
Varying loading	r_n	r_m	r_a	r_b	M	T	T	T	T
Constant loading	T	T	T	T	T	r_n	r_m	r_a	r_b

^aOnly compatible with beam, plate or shell elements

summarized in Table 1. The developed program has to be able to automatically switch from a given loading state to any other one at every moment in order to respect the loading sequence given by the user. This is done by updating the boundary conditions depending on the type of elements and the type of the next loading state. In addition, the final fields of a given loading state are taken to be the initial fields for the next loading state.

For the loading states 1 to 6 and a model using 1D plane strain elements (plane strain beams), the considered set of boundary conditions is shown in Fig. 4. The boundary conditions noted B.C.a and B.C.d allow to impose a given bending angle α . The boundary condition B.C.b corresponds to a distributed force equivalent to the contact pressure that would occur when the sheet is bent in tension around a cylinder. Finally, the boundary condition B.C.c simply corresponds to horizontal component of the tensile force T to impose. The detail of each boundary condition is given in Table 2.

Considering Eq. 2, the bending angle α is directly linked at any time to the neutral surface radius r_n by:

$$\alpha = \frac{l_0}{r_n} \tag{3}$$

Thus, if one needs to vary r_n (loading state 1) or to keep it constant (loading state 6), the corresponding angle α to be imposed is determined from Eq. 3. If the bending loading has to reach a given value of r_m (loading state 2), the same set of boundary conditions is used with a progressive modification of α until the desired value of r_m is reached. The same approach is used to reach a given value of M (loading state 5) as well as for r_a and r_b (loading states 3 and 4).

When r_m , r_a or r_b has to remain constant while T varies, another set of boundary conditions is imposed as shown

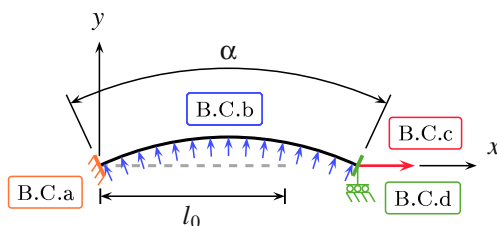


Fig. 4 Configuration of the boundary conditions for 1D plane strain elements in the case of loading states 1 to 6

Table 2 Details of the boundary conditions for 1D plane strain elements

B.C.a	Fully fixed node in both x and y directions, with a non zero angle of rotation about z set to $\alpha/2$
B.C.b	Nodal force field (considering n the number of nodes and $X(N_i)$ the initial horizontal position of node N_i): $F_x(N_i) = \frac{\alpha T}{n} \sin\left(\frac{\alpha X(N_i)}{2l_0}\right);$ $F_y(N_i) = \frac{\alpha T}{n} \cos\left(\frac{\alpha X(N_i)}{2l_0}\right).$
B.C.c	Horizontal tensile force corresponding to $F_x = T \cos\left(\frac{\alpha}{2}\right)$
B.C.d	Zero vertical displacement and constrained rotation set to $-\alpha/2$.
B.C.e	Rotation of $\alpha/2$ about z direction.
B.C.f	Nodal displacement field ensuring the desired value of r_m : $U_x(N_i) = r_m \left[\sin\left(\frac{\alpha X(N_i)}{l_0} - \frac{\alpha}{2}\right) + \sin\left(\frac{\alpha}{2}\right) \right] - X(N_i);$ $U_y(N_i) = r_m \left[\cos\left(\frac{\alpha X(N_i)}{l_0} - \frac{\alpha}{2}\right) - \cos\left(\frac{\alpha}{2}\right) \right].$ <p>For the states 8 and 9, one can simply consider $r_m = r_a + \frac{h_0}{2} \text{ and } r_m = r_b - \frac{h_0}{2}.$ </p>
B.C.g	Rotation of $-\alpha/2$ about z direction.

in Fig. 5. This time, all displacement degrees-of-freedom are controlled though B.C.f to ensure the desired bending radius. Furthermore, B.C.e and B.C.g ensure the homogeneity of the bending moment on each side. The desired value of tensile force is indirectly reached by progressively changing the value of α .

The described boundary conditions are dedicated to 1D plane strain model. If the slice is modeled with 2D plane strain elements, the boundary conditions corresponding to loading states 1 to 6 are given in Fig. 6 and detailed in Table 3. The boundary condition B.C.a allows us to impose the bending angle α through a linear relation on displacements. To ensure the planarity of the other side, an equality of horizontal displacement condition B.C.b is imposed

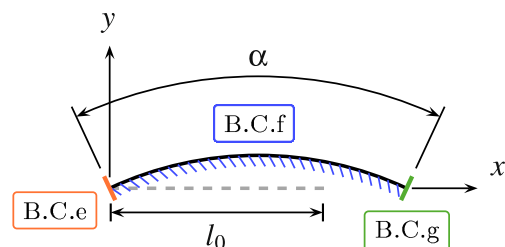


Fig. 5 Configuration of the boundary conditions for 1D plane strain elements in the case of loading states 7, 8 and 9

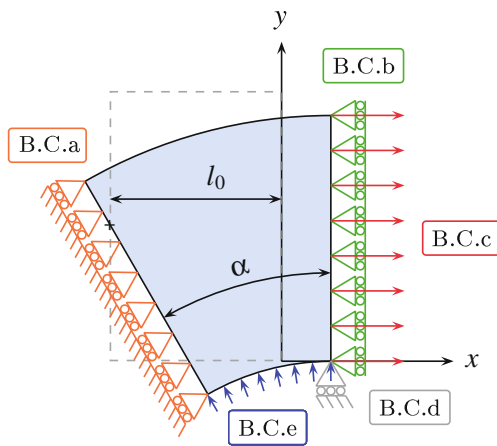


Fig. 6 Configuration of the boundary conditions for 2D plane strain elements in the case of loading states 1 to 6

between all the nodes of the face. In addition, the tensile force is uniformly distributed on the same set of nodes through B.C.c. Again, the force field B.C.e imposed on the lower or upper side corresponds to normal contact reactions. By default we select the lower surface if $\alpha T > 0$ and vice versa, which orients the force field toward the slice. Finally, zero vertical displacement is prescribed on the lower right corner node in order to avoid any rigid body movements, especially when α is close or equal to 0.

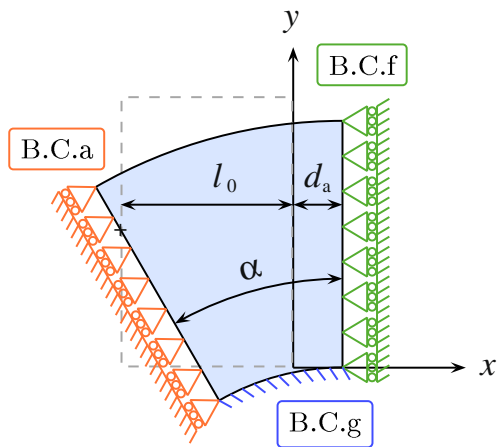
When r_a or r_b has to remain constant, boundary conditions are switched to the ones shown in Fig. 7. To maintain r_a (respectively r_b) constant, the lower (upper) surface displacements will be fully controlled through the boundary condition B.C.g (B.C.i). The horizontal displacement d_a (respectively d_b) imposed through B.C.f (B.C.h) to the right side is directly linked to α and the radius r_a (r_b). The desired value of the tensile force is indirectly reached by progressively changing the value of α . Finally, the corrective weighting δ used in boundary conditions B.C.h and B.C.i aims to maintain $U_y(N_0)$ close to 0. It corresponds to the thinning $r_b - r_a - h_0$ measured at the end of the previous step. Thus, large vertical displacements will be avoided while switching from the loading state reference 9 to an other one.

If 3D solid or solid-shell elements are preferred, the same type of boundary conditions as those given for 2D plan strain elements can be used. Only additional fixed displacements to respect the plane strain state are needed in direction z on each node N_i belonging to the front and rear sides. Likewise, boundary conditions established for 1D plane strain elements can be used on a 2D plate or shell element type with additional symmetry conditions on the front and rear sides. So far, the slice width w_0 was assumed to be the same as the sheet width W_0 . If $w_0 \neq W_0$, the tensile force and bending moment applied to the slice must naturally be reduced by a factor of W_0/w_0 .

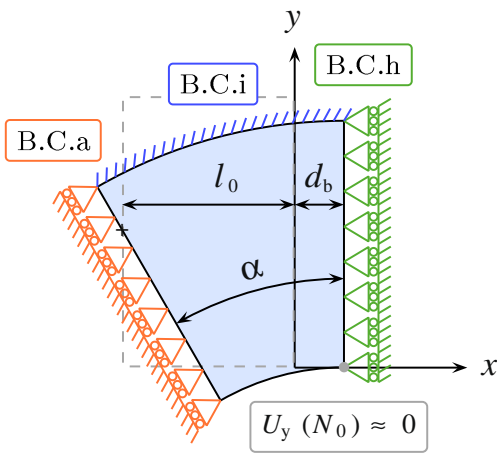
Table 3 Details of the boundary conditions for 2D plane strain elements

B.C.a	Linear relation between U_x and U_y : $U_x(N_i) = \left[\frac{h_0}{2} - Y(N_i) - U_y(N_i) \right] \tan \alpha$ where $Y(N_i)$ is the initial vertical position of node N_i .
B.C.b	Horizontal displacement equality between all nodes of the considered boundary: $U_x(N_i) = U_x(N_j)$.
B.C.c	Tensile forces T uniformly distributed: $F_x(N_i) = T/n_1$ where n_1 is the number of nodes on the left side.
B.C.d	Vertical zero displacement on one single node N_0 to avoid any rigid body movements.
B.C.e	Nodal force field (considering n_2 the number of nodes on the bottom surface and $X(N_i)$ the initial horizontal position of node N_i): $F_x(N_i) = \frac{\alpha T}{n_2} \sin \left(\frac{\alpha X(N_i)}{l_0} \right);$ $F_y(N_i) = \frac{\alpha T}{n_2} \cos \left(\frac{\alpha X(N_i)}{l_0} \right).$ If needed, this force field can be imposed on the upper surface instead of the lower one.
B.C.f	Horizontal displacement d_a imposed on the left side: $U_x(N_i) = d_a = \left(r_a + \frac{h_0}{2} \right) \tan \alpha - l_0.$
B.C.g	Nodal displacement field ensuring the desired value of r_a : $U_x(N_i) = r_a \sin \left(\frac{\alpha X(N_i)}{l_0} \right) - X(N_i) + d_a;$ $U_y(N_i) = r_a \left[\cos \left(\frac{\alpha X(N_i)}{l_0} \right) - 1 \right].$
B.C.h	Horizontal displacement d_b imposed on the left side: $U_x(N_i) = d_b = \left(r_b - \frac{h_0}{2} - \delta \right) \tan \alpha - l_0$ where δ corresponds to the thinning $r_b - r_a - h_0$ measured at the end of the previous step.
B.C.i	Nodal displacement field ensuring the desired value of r_b : $U_x(N_i) = r_b \sin \left(\frac{\alpha X(N_i)}{l_0} \right) - X(N_i) + d_b;$ $U_y(N_i) = r_b \left[\cos \left(\frac{\alpha X(N_i)}{l_0} \right) - 1 \right] - \delta.$

Regardless of its type, a single element is sufficient in the length direction x (as well as in width direction z if applicable) by taking $l_0 \ll L_0$. Such a configuration may be seen as a reduction of the dimensionality of the model, since the 3D/2D model is transformed into a 2D/1D model. In the y direction, n solid elements are needed across the thickness or even a single element if a beam, plate or shell is selected. In all cases, the number of elements is greatly decreased. Consequently, the computation time is significantly reduced compared to a finely meshed complete model of length L_0 , while the accuracy remains the same for a given type and



Loading state 8



Loading state 9

Fig. 7 Configuration of the boundary conditions for 2D plane strain elements in the case of loading states 8 and 9

size of elements due to homogeneity of local kinematics in the length direction.

Analytical part: from the B-U-T model to the deep drawing model

The model reduction approach is composed of three main steps as described below. The first step consists of identifying the number of regions constituting the formed sheet where the loading can be assumed as homogeneous in the length direction. We note that only the number of regions has to be identified here and that their size is irrelevant at this stage.

Then, the loading path associated to each region is established at the second step. This loading paths are applied

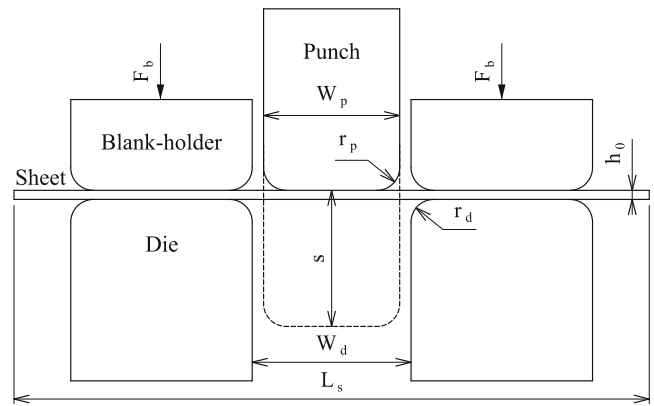


Fig. 8 Geometrical parameters considered for the U-shaped sheet

thanks to the bending-under-tension model which operates at a single section at a time, as described in the previous paragraph.

Finally, the whole model is integrated and the springback shape is reconstructed at the last step of this approach.

To illustrate each step, a standard U-shaped sheet [15] is taken as an example. Figure 8 shows the geometrical parameters considered from this point on.

First step: identification of homogeneous regions

The first step consists of identifying on the expected profile, the number of regions where loading path can be assumed as homogeneous in the length direction. This type of reduction has already been used in other analytical approaches (e.g. Zhang et al. [20]). For the U-shaped sheet, we consider five regions as shown in Fig. 9. Due to symmetry, only one

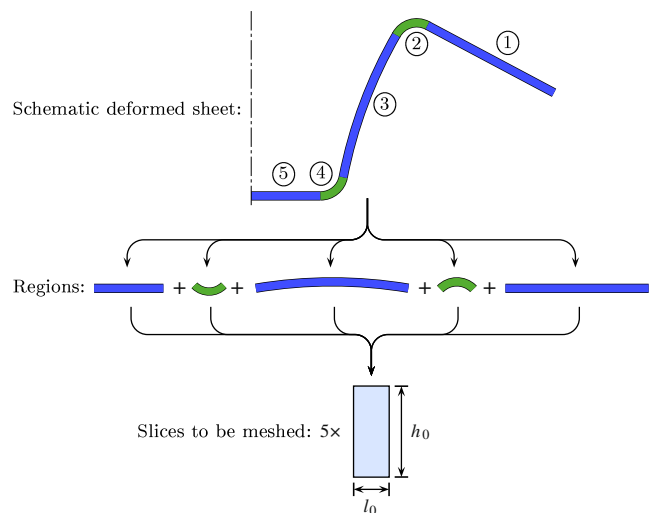


Fig. 9 Schematic representation of the five homogeneous regions considered for the U-shaped sheet, and the five corresponding slices. Actual springback shape does not need to be known in advance, neither the initial length of each considered region

half of the profile is shown. Note that the actual shape of the deformed sheet does not need to be known in advance. The actual size and shape of each considered region will

be determined later, in the reconstruction step of the present approach.

Second step: loading path

The loading path prediction is of major importance since it has a significant impact on the result. The loading states occurring during the forming phase of the U-shaped example are given in Fig. 10.

In many cases, the plastic strains occurring in the first region (the one located under the blank-holder) can be neglected. Then, its final shape is the same as the initial one, regardless of the loading path. This assumption is made for the U-shaped example, thus only slices 2 to 5 need to be modeled. Table 4 summarizes the considered loading sequence of each slice to model. The times t_4 and t_5 correspond to the springback phase, that is a zero tensile force and a zero bending moment. During the forming phase, all slices to be modeled are submitted to non zero tensile forces, T_2 to T_5 , the values of which need to be determined.

The blank-holder acting on the first region will generate the main part of the tensile loading transmitted to regions 2 to 5. Assuming a Coulomb friction, the tensile force generated in the sheet due to friction with the blank-holder corresponds to:

$$T_0 = \mu F_b \tag{4}$$

where μ is the friction coefficient and F_b the blank-holder force.

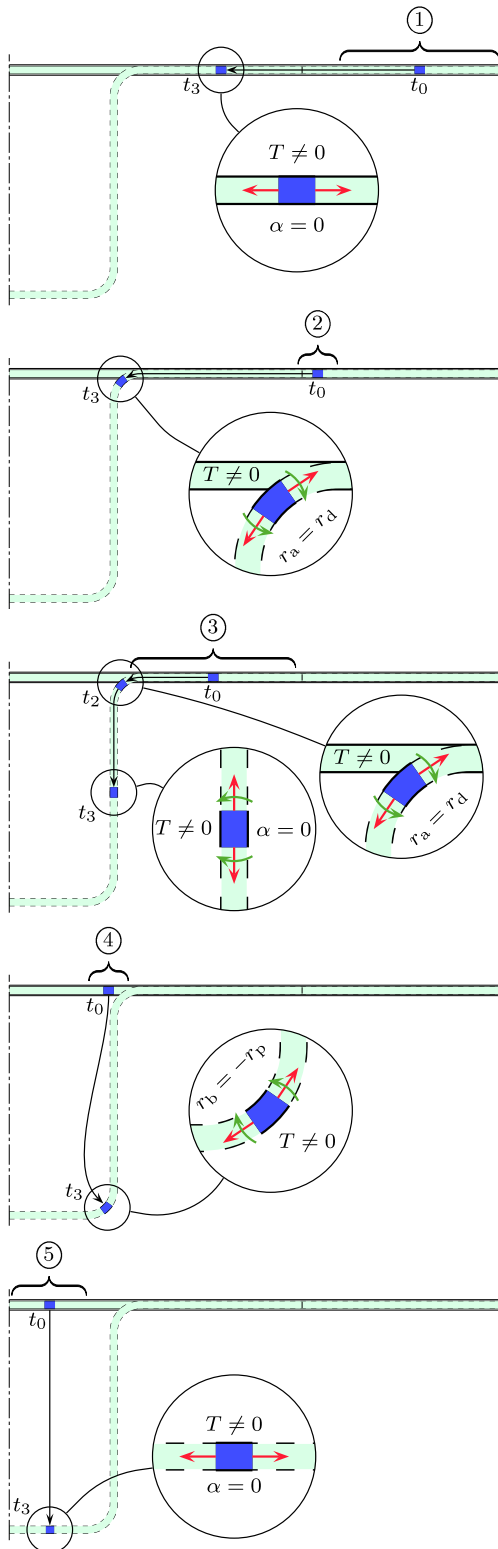


Fig. 10 Loading states of each considered slice occurring during the forming phase (from time t_0 to time t_3)

Table 4 Loading sequences considered for the U-shaped sheet

Time	t_1	t_2	t_3	t_4	t_5
Loading sequence for the slice 2					
Loading state		6	3	8	5
Varying loading		$T = T_2$	$r_a = r_d$	$T = 0$	$M = 0$
Constant loading		$r_n = \infty$	$T = T_2$	$r_a = r_d$	$T = 0$
Loading sequence for the slice 3					
Loading state	6	3	2	6	5
Varying loading	$T = T_3$	$r_a = r_d$	$r_n = \infty$	$T = 0$	$M = 0$
Constant loading	$r_n = \infty$	$T = T_3$	$T = T_3$	$r_n = \infty$	$T = 0$
Loading sequence for the slice 4					
Loading state		6	4	9	5
Varying loading		$T = T_4$	$r_b = -r_p$	$T = 0$	$M = 0$
Constant loading		$r_n = \infty$	$T = T_4$	$r_b = -r_p$	$T = 0$
Loading sequence for the slice 5					
Loading state			6	6	
Varying loading			$T = T_5$	$T = 0$	
Constant loading			$r_n = \infty$	$r_n = \infty$	

The same tensile force is generated by friction between the first region and the die. Thus, the total tensile force induced by the blank-holder is given by:

$$T_1 = 2T_0 \tag{5}$$

The region 2 is bent around the die radius r_d . As introduced in bending under tension tests by [10], exponential friction occurs in this region and the tensile force reached in region 3 is approximately given by:

$$T_3 = T_1 \times e^{\mu\pi/2} \tag{6}$$

The tensile loading considered for region 2 will be simply taken as the average of regions 1 and 3:

$$T_2 = \frac{T_1 + T_3}{2} \tag{7}$$

In addition to the tension T_3 , the region 3 will be bent with a curvature radius r_d , then unbent along the die side-wall. The region 4 will go through the same type of loading as region 2 with the tension $T_4 = T_3$ and a negative bending radius corresponding to the punch radius r_p . Finally the bending of region 5 will be neglected and only the tension will be considered that is $T_5 = T_3$.

Last step: reconstruction of the global shape after springback

At first, the initial length L_0 of each region has to be determined from the state corresponding to the end of the loading phase (time t_1) just before the springback phase (completed at t_2). For curved regions at t_1 of angle $A(t_1)$, L_0 corresponds to:

$$L_0 = A(t_1) \cdot r_n(t_1) = A(t_1) \frac{l_0}{\alpha(t_1)} \tag{8}$$

For the U-shaped example, only regions 2 and 4 are curved at t_1 with angles $A(t_1) = \frac{\pi}{2}$ and $A(t_1) = -\frac{\pi}{2}$ respectively. For flat regions at t_1 of elongation corresponding to $d(t_1)$, the initial length is given by:

$$L_0 = L(t_1) \frac{l_0}{l_0 + d(t_1)} \tag{9}$$

For the concerned regions 3 and 5, the values of $L(t_1)$ are taken as $L(t_1) = s - h_0 - r_p - r_d$ and $L(t_1) = \frac{W_p}{2} - r_p$ respectively.

Then the final angle $A(t_2)$ for curved regions after springback and the final length $L(t_2)$ for flat ones can be determined as:

$$A(t_2) = L_0 \frac{\alpha(t_2)}{l_0} \tag{10}$$

$$L(t_2) = L_0 \frac{l_0 + d(t_2)}{l_0} \tag{11}$$

Only region 5 of the U-shaped sheet is flat at t_2 while regions 2, 3 and 4 are curved. For these curved regions, we finally need to extract $r_m(t_2)$ in order to reconstruct

the whole springback profile. The remaining length of the region 1 will be deduced from the other regions by subtracting their initial lengths from the total initial sheet length L_s (Fig. 8).

Application of the proposed approach

U-shaped sheet

As a first test case, we apply the proposed approach to the example of the U-shaped sheet discussed above. The bending-under-tension model was programmed using the implicit finite element software Code_Aster [8] with large strain formulation. The mechanical behavior of the blank is considered as simply isotropic elastic-plastic with a linear kinematic hardening based on the von Mises criteria. The material properties as well as the geometrical and loading parameters are listed in Table 5. A friction coefficient of 0.15 was taken into account between the blank and the tools considered as being rigid.

Each slice was modeled with a single shell element (Discrete Kirchhoff Quadrangle formulation). Its dimensions were set to $l_0 = 1$ mm and $w_0 = 1$ mm. In the thickness direction, 10 integration points were used. In order to assess the accuracy of the reduced model, a comparison was made with the result obtained from a complete deep drawing simulation performed in dynamic explicit mode by the finite element software LS-DYNA [11], using Belytschko–Tsay shell element formulation and 10 through thickness integration points with the same behavior law and parameters (5). Both predicted shapes after springback are reported on Fig. 11. A moderate shift is observed on the reduced model shape compared to the complete modeling taken as reference.

Table 5 U-shaped sheet geometrical parameters and material properties (for isotropic elastic-plastic material with a linear kinematic hardening based on the von Mises criteria)

Geometry		Material	
L_s	300 mm	E	70.5 GPa
h_0	0.8 mm	ν	0.342
W_s	1 m	ρ	2700 kg/m ³
W_p	60 mm	σ_y	180 MPa
r_p	10 mm	H	1.5 GPa
W_d	62 mm		
r_d	10 mm		
Loading		Contact	
F_b	300 kN	μ	0.15
s	60 mm		

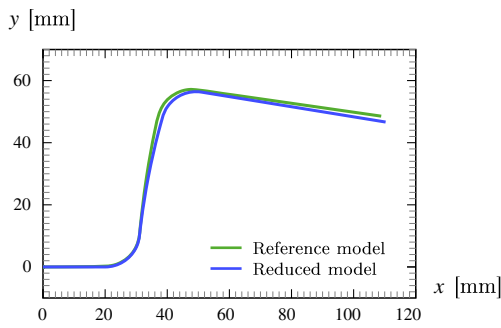


Fig. 11 Comparison of the predicted shape after springback for the U-shaped sheet

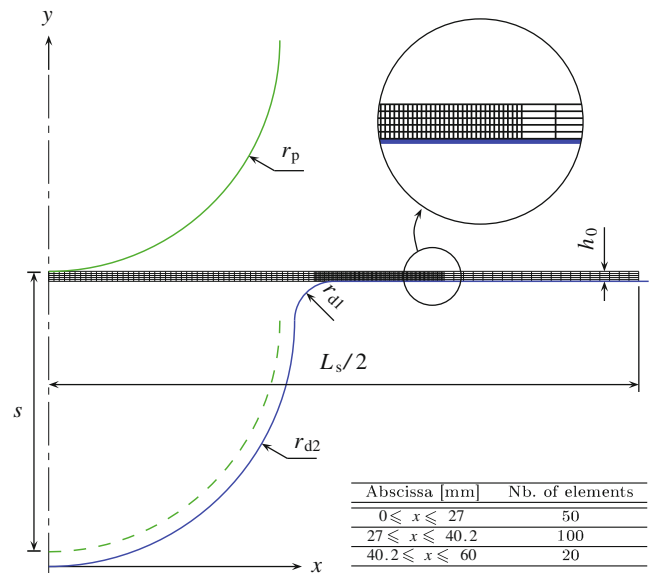


Fig. 13 Finite element mesh and geometrical parameters of the reference model of cylindrical bending

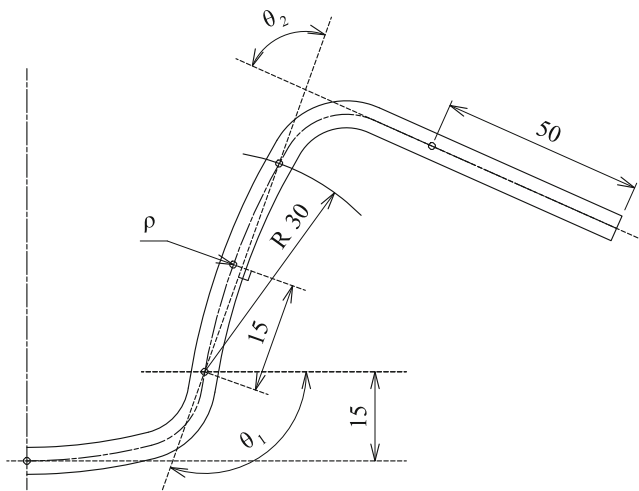


Fig. 12 Detail of the springback parameters on a schematic U-channel profile

Table 6 Springback parameters predicted by the proposed approach compared to the reference result

Model	θ_1	ρ	θ_2
Reference model	98.88°	295.8 mm	90.71°
Reduced model	101.14°	232.8 mm	91.9°
Difference	2.28 %	21.3 %	1.31 %

To quantify this difference, springback parameters were measured as defined in Fig. 12. These measures are reported in Table 6. The radius of curvature ρ presents the main difference, exceeding 20 %, which is not that obvious on the graphic representation, especially because sidewall curl is moderate in the present case. The two springback angles θ_1 and θ_2 are relatively attained with a maximum error of 2.28 %.

Unconstrained cylindrical bending

The second example consists of cylindrical bending without any blank-holders. This deep drawing test was initially proposed at Numisheet 2002, benchmark B problem [5]. Code_Aster was used to compute both the reference and the reduced model. This time, 8 node 2D plane strain

Table 7 Cylindrical bending geometrical parameters and material properties

Geometry		Material	
L_s	120 mm	E	70.5 GPa
h_0	1 mm	ν	0.342
r_p	23.5 mm	ρ	2700 kg/m ³
r_{d1}	4 mm	σ_y	194 MPa
r_{d2}	29 mm	K	550.4 GPa
		n	0.223
Loading		Contact	
s	28.5 mm	μ	0.1342

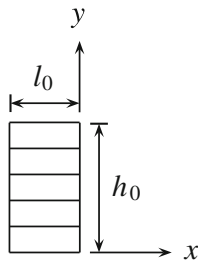


Fig. 14 Finite element mesh of a reduced model slice constituted of a single column of 5 elements

Table 8 Loading sequence imposed to the slice of the reduced model

Time	t_1	t_2
Loading state	3	5
Varying loading	$r_a = -r_p$	$M = 0$
Constant Loading	$T = 0$	$T = 0$

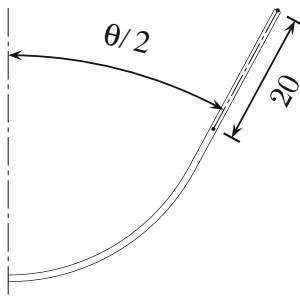


Fig. 15 Definition of the blank angle θ needed at t_1 and t_2

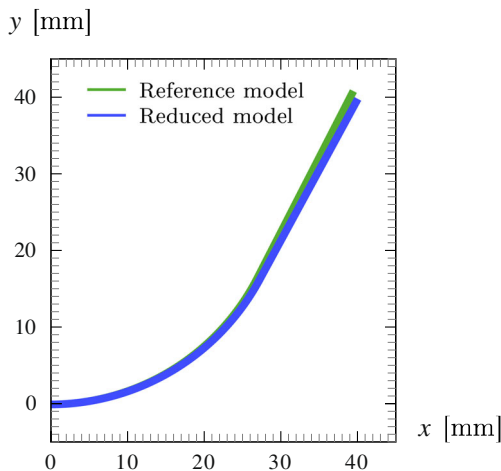


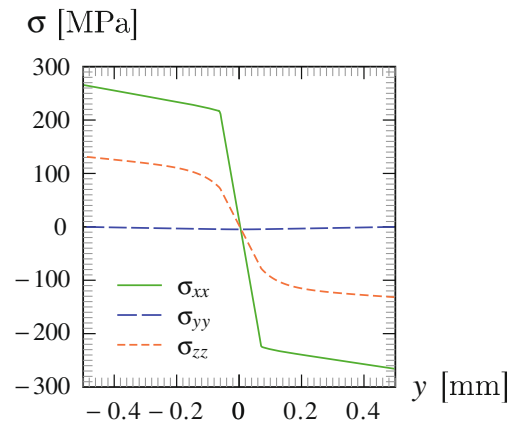
Fig. 16 Comparison of the predicted shape after springback of the bent sheet

Table 9 Springback parameters predicted by the proposed approach compared to the reference result

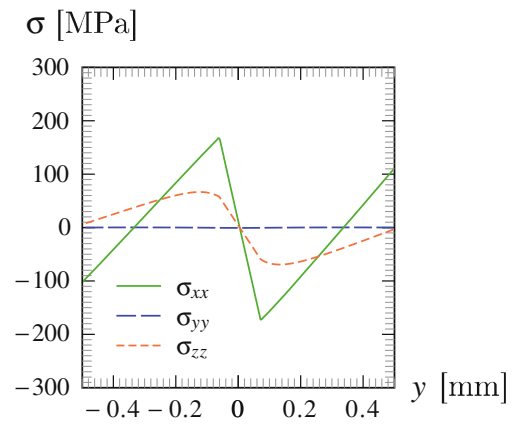
Model	$\theta(t_2)$
Reference model	54.28°
Reduced model	56.94°
Difference	4.9 %

quadratic elements were selected for each modeled slice. The isotropic elastic-plastic blank, with Hollomon’s hardening law based on the von Mises criteria, is the same as in [13]. The mesh used for the reference model is shown in Fig. 13. The corresponding data and geometric parameters are listed in Table 7.

In the reduced model, only the region in contact with the punch needs to be modeled. As for the reference model, 5 elements were used through the thickness with the same length that is $l_0 = 0.54$ mm (Fig. 14). The 2 extremities are assumed to remain flat during the whole process while the



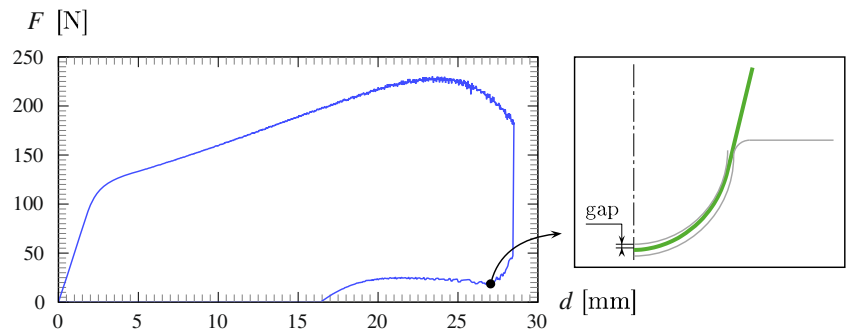
At the end of the forming phase



After springback

Fig. 17 Reduced model stress evolutions through the thickness expressed in the local basis and centered on the mean surface

Fig. 18 Punch force versus displacement and deformed shape at the beginning of the unloading phase



center region is bent with a upper radius $r_b = -r_p$ and then unloaded that is $M = 0$. No any tensile force is taken into account. The loading sequence is summarized in Table 8.

For the reconstruction step of the shape after springback, one needs to know the bending angle $A(t_1)$ which corresponds to:

$$A(t_1) = \theta(t_1) - \pi \tag{12}$$

where $\theta(t_1)$ is the angle formed by the blank (Fig. 15) when the punch reaches the depth s and can be approximated by:

$$\theta(t_1) = 2 \cdot \left[\arctan \left(\frac{r_p + h_0 + r_{d1} - s}{r_{d1} + r_{d2}} \right) + \arccos \left(\frac{r_p + h_0 + r_{d1}}{\sqrt{(r_p + h_0 + r_{d1} - s)^2 + (r_{d1} + r_{d2})^2}} \right) \right] \tag{13}$$

By applying this relation to the present case, we find that $\theta(t_1) \simeq 21.31^\circ$. Knowing $A(t_1)$ from $\theta(t_1)$, the relations (8) and (10) are successively used to finally determine the springback shape and its characterizing angle:

$$\theta(t_2) = \pi + A(t_2) \tag{14}$$

The deformed shape predicted by the proposed semi-analytical model as well as the one given by the reference model are shown in Fig. 16. The angle $\theta(t_2)$ formed by the 2 straight sides of the sheet after release is higher for the reduced model than the reference one. The predicted values, varying by 4.9 % between the 2 versions, are reported in Table 9.

Since the reduced model involves a negligible computing time, the number of elements across the thickness was changed from 5 to 200 without falling into prohibitive CPU time. The stress evolutions given by the reduced model with 200 elements are shown in Fig. 17, at the end of the forming phase and after springback. The springback angle decreased

slightly to reach 56.89° . The same mesh refinement was not applied to the reference model due to the prohibitive computing time involved. But since the reduced model shows a very low variation, one can make a reasonably assumption that 5 elements in the thickness direction are sufficient in both cases.

The analysis of the reference model indicates that a gap appears at the beginning of the unloading phase, between the punch and the blank as shown in Fig. 18. The loading path becomes slightly different from the one assumed for the reduced model. It can be shown that this is the main source of error. Indeed, if the 2 first nodes in contact between the punch and the blank are merged to avoid any gap formation, then the springback angle increases to 56.64° while the difference with the reduced model decreases to 0.5 %.

Conclusions and perspectives

The proposed numerical model of bending-under-tension allows us to determine the mechanical state of a bent sheet with a possibly additional tension assuming a plane strain state. Due to the limited number of elements needed, the simulations are completed in a short computation time. Moreover, this numerical model presents some advantages compared to analytical ones. Indeed, one can directly use any material behavior laws already present in legacy finite element codes, unlike analytical approaches that are mainly based on simplified mechanical behavior with assumption of incompressibility. Analytical approaches are also frequently limited to small strains and to a single bending-unbending cycle, while the proposed semi-analytical approach allows us to perform several cycles with large strains. This numerical bending-under-tension model is also independent of the geometry of the considered deep-drawn part.

The B-U-T model is able to automatically switch between the appropriate boundary conditions in order to respect the selected loading path. Hence, the semi-analytical deep-drawing approach has the advantage that no any

description of the boundary conditions has not to be re-developed for each geometry. In the given test cases, a limited error is naturally observed in comparison with reference models. This error is mainly explained by shear stresses which are neglected as well as by loading paths which are simplified and considered to be homogeneous in each region constituting the formed sheet. Thus, in order to validate or refine the results given by the reduced model approach, a complete simulation should be performed. This approach could also be used to optimize the deep drawing process with various methods combined to the reduced model proposed in this paper. As shown for the cylindrical bending example, the model provides a simple alternative way to determine the number of elements or through-thickness integration points needed for a full-scale simulation.

The semi-analytical approach of plane strain deep drawing based on the numerical B-U-T model constitutes an attractive alternative tool to assess springback. It can also be used in to assess the evolution of the various fields after springback or during the whole operation versus the input parameters, in a short computation time. For a typical plane strain deep drawing, we have reduced the computation time by two orders of magnitude. Thus, this approach opens the way to perform stochastic analysis by Monte-Carlo type approaches and this is the subject of the undergoing work.

Furthermore, if the width of the blank is small compared to its thickness, a plane stress condition may occur. In such a situation, the bending-under-tension model may still be used with few modifications to switch from plane strain to plane stress condition. Sections other than rectangular are also possible, since the steps of the reduced model approach remaining the same.

Finally, for future work, the proposed approach could be used to develop a reduced model of draw-bead for optimization purposes within limited design time. This approach may also be used for flattener processes as well as sheet metal folding, wiping, roll bending and other plane strain forming cases, assuming a complex visco-elastic-plastic behavior, with damage evolution and/or involving anisotropic properties. Some improvements to take into account a combined shear stress or a biaxial bending-under-tension load will also permit us to extend the scope of this approach and to decrease the error as compared to a complete simulation.

Acknowledgments This research was conducted as part of the OASIS project, supported by OSEO within the contract FUI no. F1012003Z.

The authors acknowledge the support of Labex MS2T.

References

- Alexandrov S, Hwang YM (2009) The bending moment and springback in pure bending of anisotropic sheets. *Int J Solids Struct* 46:4361–4368
- Alexandrov S, Manabe K, Furushima T (2011) A general analytic solution for plane strain bending under tension for strain-hardening material at large strains. *Arch Appl Mech* 81:1935–1952
- Asnafi N (2000) Springback and fracture in v-die air bending of thick stainless steel sheets. *Mater Des* 21:217–236
- Breitkopf P, Naceur H, Rassineux A, Villon P (2005) Moving least squares response surface approximation: formulation and metal forming applications. *Comput Struct* 83:1411–1428
- Brem JC, Barlat F, Fridy JM (2002) Free bending benchmark testing of 6111-T4 aluminium alloy sample. In: *Numisheet Conference, Korea*
- Bruhns OT, Gupta NK, Meyers ATM, Xia H (2003) Bending of an elastoplastic strip with isotropic and kinematic hardening. *Appl Mech* 72:759–778
- Buranathiti T, Cao J (2004) An effective analytical model for springback prediction in straight flanging processes. *Int J Mater Prod Technol* 21:137–153
- Code.Aster (2009) Analysis of structures and thermomechanics for studies & research. EDF-R&D
- Da Silva Botelho T, Bayraktar E, Inglebert G (2006) Comparison of experimental and simulation results of 2D-draw-bend springback. *J Achiev Mater Manuf Eng* 18:275–278
- Duncan J, Shabel B, Filho J (1978) A tensile strip test for evaluating friction in sheet metal forming. *Tech. rep., SAE Technical Paper* 780391
- Hallquist JO (2006) *LS-DYNA theory manual*. Livermore Software Technology Corporation
- Hill R (1950) *The mathematical theory of plasticity*. Clarendon Press, Oxford
- Konter AWA (2005) *Advanced finite element contact benchmarks*. Tech. Rep., FENET
- Lee MG, Kim D, Wagoner RH, Chung K (2007) Semi-analytic hybrid method to predict springback in the 2D draw bend test. *J Appl Mech* 74:1264–1275
- Makinouchi A, Nakamachi E, Onate E, Wagoner RH (1993) Guide to the benchmark test—simulation and experiment. In: *Numisheet'93 conference, The Institute of Physical and Chemical Research*, pp 32–39
- Naceur H, Delaméziere A, Batoz JL, Guo YQ, Knopf-Lenoir C (2004) Some improvements on the optimum process design in deep drawing using the inverse approach. *J Mater Process Technol* 146:250–262
- Parsa M, Nasher AI Ahkami S (2008) Bending of work hardening sheet metals subjected to tension. *Int J Mater Form* 1:173–176
- Pourboghrat F, Chung K, Richmond O (1998) A hybrid membrane/shell method for rapid estimation of springback in anisotropic sheet metals. *J Appl Mech* 65:671–684
- Sun G, Li G, Zhou S, Xu W, Yang X, Li Q (2011) Multi-fidelity optimization for sheet metal forming process. *Struct Multidiscip Optim* 44:111–124
- Zhang D, Cui Z, Ruan X, Li Y (2007) An analytical model for predicting springback and side wall curl of sheet after u-bending. *Comput Mater Sci* 38:707–715
- Zhu HX (2007) Large deformation pure bending of an elastic plastic power-law-hardening wide plate: analysis and application. *Int J Mech Sci* 49:500–514